Near surface transformations of stainless steel cold spray and laser cladding deposits after turning and ball-burnishing

C. Courbon, A. Sova, F. Valiorgue, H. Pascal, J. Sijobert, G. Kermouche, Ph. Bertrand, J. Rech

Near surface transformations of stainless steel cold spray and laser cladding deposits after turning and ball-burnishing

C. Courbon[a], A. Sova[a,*], F. Valiorgue[a], H. Pascal[a], J. Sijobert[a], G. Kermouche[b], Ph. Bertrand[a], J. Rech[a]

[a] *Univ Lyon, ENISE, ECL, ENTPE, CNRS, LTDS UMR 5513, F-42023, Saint-Etienne, France*
[b] *Univ Lyon, Ecole des Mines de Saint-Etienne, CNRS, LGF UMR5307, F-42000, Saint-Etienne, France*

Abstract

An experimental study is performed to assess the surface integrity of cold sprayed and laser cladded 17-4PH stainless steel deposits after turning and ball-burnishing. A special emphasis is given to near surface microstructure and residual stress distribution. It is shown that both cold spray and cladding deposits could be machined under cutting conditions close to those employed for a conventionally rolled 17-4 PH stainless steel. Analysing the resulting microstructure in the near-surface revealed that the turning and ball-burnishing processes affect the coating surface and generate a thin layer where the microstructure can be hardly identified. Residual stress measurements by an X-ray diffraction method revealed that turning results in tensile residual stresses in the near-surface of both the cold spray and laser cladding deposits. Surface treatment by ball-burnishing can be significantly beneficial as compressive residual stresses were measured in both coatings in the near-surface zone but to a larger extent in the cladded material. The comparison of the two profiles showed that the cutting and deformation mechanisms can be significantly different depending on the intrinsic nature of the deposited microstructure.

Keywords: Cold spray, laser cladding, surface integrity, microstructure, residual stresses

*Corresponding Author. Tel.: +33 4 77 43 75 72
Email address: aleksey.sova@enise.fr (A. Sova)

1. Introduction

In many industrial applications including metallurgy, nuclear, aerospace or mining industries, extreme working conditions can lead to the early failure of mechanical components. In order to avoid catastrophic consequences, regular maintenance and often advance replacement of the concerned component have to be carried out. If optimizing the design of the latter or the composition/microstructure of its basis material were the preferred strategies, applying an overlay onto a core material appeared as a promising solution. This is not only true for new high added-value functional parts but also as an alternative method to repair the used ones. Recent advances in coatings and thermal-spaying technologies indeed made it possible by the deposition of films with enhanced wear [1, 2] or corrosion resistance [3, 4] and fatigue properties [5, 6]. As far as repairing is concerned, thick deposits are especially sought-after leading to the use of relevant processes such as flame [7] or High Velocity Oxy-Fuel (HVOF) spraying [8], welding [9], but also laser processes [10, 11] or even recently cold spray [12, 13].

Laser cladding (LC) is a high temperature material deposition technology where the powder material is transported by an inert gas toward a molten pool created by a laser beam. After a melting phase, the material rapidly solidifies forming a bead with a thickness that can exceed 2mm and a width up to 5mm [14]. The powder can be delivered to the substrate either laterally or coaxially with the laser beam. In the latter configuration, particles reach the base material with a higher temperature due to a longer interaction time while travelling into the laser beam. A thick coating can thus be generated by overlapping successive cladding beads. On one hand, LC is known to be a flexible but also an efficient deposition method because of the dilution of the coating into the substrate resulting in a strong metallurgical bond [15]. On the other hand, LC being based on successive melting and solidification of the deposited material, tensile residual stresses develop due to the high thermal gradients involved and differential thermal expansions [16, 17, 18]. Stress-relieving heat treatments are therefore required to ensure the functionality of the coating [19].

Cold Spray (CS) is a deposition process in which the powder particles are accelerated in a high-speed gas flow delivered by a supersonic nozzle [20, 21]. The particle velocity is a key parameter governing the impact energy and leading or not to a severe plastic deformation of both particle and substrate surfaces [22]. Oxide films formed on each of them being broken after the impact, a strong bonding is achieved via the new chemically active surfaces [23]. One specificity of CS compared to many thermal spraying techniques, is the relatively low deposition temperature which does not exceed the powder melting temperature. This of course avoids melting of the deposited material but most of all oxidation or crystallization. One of the main advantages of cold spray resulting in this low temperature is the possibility to produce very thick deposits due to the relatively low level of residual stresses induced in the sprayed layers [24].

These two techniques have been proved to be efficient in producing various deposits such as functional-

gradient [25, 26], composites [27, 28] or multi-layer ones [29, 30]. Moreover, there is currently a growing trend for using these deposition techniques not only for coatings or repairing but also for the direct manufacturing of functional components, i.e. as additive manufacturing processes. Both cold spray and laser cladding are being explored as viable solutions especially due to their free-form fabrication capabilities, fine deposition resolution and the possibility to build parts based on a layer-by-layer deposition. More than ten years ago, Blose et al [31] and Pattison et al [32] were the first authors to reports that cold spray appeared as a promising additive manufacturing technique. Several lastly published works[33, 34, 35] confirmed this trend and showed the great potential of cold spray. Laser cladding is also concerned and this direct metal deposition alternative already showed some successful [36, 37, 38] However, their main drawback is that few surfaces can be directly manufactured meeting the final functional requirements in terms of dimensional accuracy, surface roughness or even surface integrity. Fine dimensional tolerances are indeed hard to achieve as the width of a spraying track is commonly larger than 1mm. Resulting surface finish can widely exceed Ra values of $50\mu m$ whereas near surface properties such as residual stresses, microstructure, hardness or porosity can be found highly detrimental. These surface and near surface properties are of primary importance as they directly govern the fatigue life of the coated or manufactured components [6, 39, 5]. Post-processing of the deposited material is then often required.

Several research works tried to apply post-treatment methods such as laser treatments to improve CS porosity [40], laser shock peening [41], laser annealing or deep rolling to modify the residual stresses distribution in LC [42]. Despite the fact that machining and superfinishing processes such as ball burnishing are widely employed in industry, really few studies investigated their effects on CS and LC deposits. Recently, Zhang et al. [43] showed how to improve the machining of LC coatings in terms of surface roughness using wiper inserts. In two others studies, the same authors focused their work on surface integrity aspects [44, 45] and highlighted the positive influence of turning and ball-burnishing on properties such as residual stresses, porosity or bonding strength. The recent work of the present authors [46] especially proved that the beneficial properties of a as-deposited CS 17-4PH coating, i.e. deep and large compressive residual stresses, can be totally lost once a machining operation is applied whereas a ball-burnishing process can partially recover them. A major benefit is that ball-burnishing can be naturally combined to a finish turning operation as the required tooling can be mounted on a standard CNC lath. This has the advantage of keeping the whole process smooth, simple and flexible without the need to mount the part on another machine or device. The later works of Chew et al. [5] and Zhang and Liu [45] especially tried to connect these coating modifications to final in-use properties such as fatigue life or corrosion resistance. These recent investigations showed the potential of applying finishing and superfinishing methods but unfortunately there is still a limited knowledge on how those can affect the mechanical and metallurgical properties of thick CS or LC coatings. Especially, no studies reported a comparison of the final properties reached for the same material deposited by two different techniques once a machining or superfinishing operation is applied.

This paper thus aims at providing a new insight into the near surface properties of thick 17-4 PH stainless steel coatings deposited by CS and LC after turning and ball-burnishing. A special emphasis is given to residual stresses distribution and subsurface microstructure as this aspect has yet not been deeply investigated in the literature.

2. Materials and Methods

2.1. Powder and Substrate

Commercial gas-atomized 17-4 PH stainless steel powder produced by TLS GmbH (Germany) was used in the different experimental campaigns. The particle size distribution are described in Figure 1a whereas the morphology of the powder is shown in Figure 1b. The powder particles are both characterized by a spherical shape with the presence of some satellites. However, the powder used in CS has a finer size (D10/D50/D90 = 10/28/43μm) compared to the one employed in LC (D10/D50/D90 = 50/69/89μm) as it can be seen in Figure 1a.

Regarding the deposition performed by Cold Spray, the substrates were made of 1050 aluminum as cylinders with an outer diameter of 50mm. Spraying was performed on the as-turned surface without any preparation procedures.

In Laser Cladding, a standard a E335 0.4% carbon non-alloy steel was selected according to the higher deposition temperatures. Cylinders with an outer diameter of 50mm were machined and no specific preparation process was applied on them before deposition.

2.2. Coating deposition parameters

Cold spray coatings were applied using a CGT KINETIKS 4000 system fitted with a Type 40 converging-diverging nozzle. The cylindrical substrates were clamped on a rotating system controlling their angular position and speed while the deposition took place with the nozzle moving parallel to the cylinder axis. Nitrogen was used as a propellant gas, and the main spraying parameters are specified in Table 1.

It has been proved that the ratio of the impact to critical velocity [47] directly govern the bonding properties of a cold spray coating and that higher impact/critical velocity ratio are beneficial. It is also possible to control the particle impact velocity by varying the gas stagnation pressure and temperature [20, 22, 23]. Therefore, the gas stagnation pressure was set to the highest possible value allowed by the system (4.0MPa) whereas the temperature selected in order to avoid the clogging of the nozzle (923K) CGT KINETIKS 4000 cold spray system. This combination was assumed to ensure the highest particles acceleration resulting in the best mechanical properties. A resulting coating thickness of 2.5mm was achieved on the as-sprayed deposits.

LC was performed on a 6-axis Trumpf Trulaser Cell 7040 cladding system equipped with a 4kW Nd-YAG laser and a 3-jets injection nozzle leading to a circular beam spot on the target surface. A 1.5mm thick coating was formed by overlapping single laser beads deposited side by side with a fixed offset of 3 mm. In order to avoid cracking at the coating/substrate interface, a stress relief heat treatment (HT) was processed in a furnace with a a holding temperature of $1035°C$ for 1 hour, oil quenched and tempered at $620°C$ for 4 hours, followed by a furnace cooling to the room temperature.

2.3. Machining and Ball Burnishing parameters

After coating deposition, both the CS and LC samples were machined by a longitudinal finish turning operation (FT). A CNMG 120408-TF IC9025 coated tungsten carbide tool was used and mounted on a PCLNL 2525M 12 tool holder, resulting in a 95° entering angle and -6° rake angle. Machining was carried out under lubrication with emulsion and the same cutting conditions were selected: Vc = 50m/min, f = 0.15mm/rev, ap = 0.3mm.

Ball burnishing (BB) was then applied on some of the coated and turned specimens. This process is a superfinishing technique that can be efficiently applied to modify the surface topography as well as the mechanical state within the near-surface layer [44, 48] (Fig. 2). A 6mm diameter ceramic ball moving on the surface with a given feed (0.05mm/rev) and speed (50m/min) is used to generate a high contact pressure. The normal load was exerted by a hydraulic pressure and controlled prior to the test under static contact conditions. A load of 250 N was then applied onto the workpiece, which is found to be common for ball burnishing of martensitic stainless steel [48].

2.4. Characterization Methods

Selected specimens have been cut, in parallel and perpendicular directions relative to the cylinder axis, mounted and polished with SiC grinding paper up to 1200 grit size followed by diamond based suspensions down to 1 μm. Porosity was estimated by image processing of these polished cross sections. Microstructural characterizations were performed after etching using a ASTM24 solution and analysed with a light optical microscope and scanning electronic microscopy (SEM). The microhardness was measured using Buehler OmniMet MHT 5104 device with Vickers indenter.

The residual stresses measurements have been performed with an X-Ray Diffraction (XRD) system equipped with a 2-mm diameter collimator with the following configuration:

- Cr Kα radiation with 18 kV, 4 mA;
- λ = 0.229 nm, planes 211;
- Bragg's angles: $2\theta = 155.00°$;
- Ω acquisition mode;

- 7 β-angles (from -30° to +30°);
- β oscillations: ±6°.

Stresses were calculated using the elliptic treatment method with the following radio-crystallographic elasticity constants: $\frac{1}{2}$ S2 = 5.92 $\times 10^{-6}$MPa^{-1}, S1 = 1.28 $\times 10^{-6}$MPa^{-1}.

The in-depth residual stress distribution has been investigated after successive layer removal using an electrochemical polishing system with a diameter of 5 mm. Electropolishing was employed to prevent a strong alteration of the initial residual stress profile.

3. Results and Discussion

3.1. Near surface microstructure

The initial microstructures and microhardnesses of the as-deposited (AD) coatings are shown in Figure 3a-b in CS and Figure 3c-d in LC.

The typical structure of a cold spray deposit can be seen on the CS-AD coating with deformed and cohered particles with residual inter-particle interfaces (Fig. 3a). A relatively low porosity has been achieved with an average value of 0.8%. The substrate/coating interface is shown in Figure 3b with stainless steel particles that strongly penetrated the aluminum substrate.

The LC coating after heat treatment exhibits a common martensitic microstructure, with a quasi equi-axis grain structure and locally slightly elongated ones towards the surface, i.e. remaining history from the growth oriented into the direction of the heat flow (Fig. 3c). Martensitic laths are visible within the prior austenitic grains whereas a specific microstructure appeared near the coating/substrate interface (Fig. 3d). Even if this is far from the region of interest, microstructural investigations showed an evolution of the typical dilution zone between the cladded material and the substrate towards a carbon-rich microstructure with a microhardness exceeding 475 HV0.1 (Fig. 4). According to the lower hardness values measured at the interface on the substrate side, 125 HV0.1 against 200HV0.1 for the bulk E335 material, a carbon diffusion from the substrate towards the 17-4PH coating via the dilution zone during the heat treatment has been assumed.

It can be noted that, with both processes, mean hardness values of the AD deposits over the first 200 μm, approx. 350-355 HV0.1 (Fig. 4), are comparable with the bulk hardness of a hot rolled 17-4 PH steel bar, heat treated under standard H 1075 conditions (340 HV.01 ± 10).

Once the two post-processing techniques were applied, the bulk microstructure of the CS coating did not appear affected as shown in Figure 5. The integrity of the coating remained without any crack, delamination or torn particles. However, focused analyses on the near-surface revealed a modified microstructure as it can

be seen in Figures 5b-c. A finish turning operation tends to cut and deform the CS particles at the surface toward the material removal direction (Fig. 5b). The particle boundaries are compressed and even become hardly visible when getting closer to the top surface. After finish turning and ball-burnishing (Fig. 5c), plastic deformation of the particles was amplified with the inter-particle boundaries highly oriented toward the material deformation direction.

Similar results have been observed on the LC coating (Fig. 6). The microstructure is transformed on 5 to 10μm from the top surface with the martensite laths deformed and oriented towards the cutting direction (Fig. 6b-c).

As these transformed thin layers deserved a deeper analysis, high resolution SEM analyses were carried out. The Figure 7 tends to show that severe plastic deformation induced by turning and ball-burnishing led to the activation of a grain refinement process due to an intense shear localisation as described in several research works [48, 49, 50]. However, this had never been clearly reported in CS or LC coatings. EBSD analyses should be performed to confirm clearly the occurrence of this phenomenon.

Surface microhardness measurements exhibit a slight variation showing that the in-depth hardness has not been affected by the two processes (Fig. 8). However, these values are the average of 3 measurements at depths from 50 to 200μm in order to avoid any boundary effect when getting closer of the top surface. Considering the thickness of the transformed layers identified in the previous figures, these slight increases reveal a modification of the in-depth properties but could significantly underestimate the hardness of the surface and near-surface region. Nanoindentation should be employed to extract their actual mechanical properties with a more local measurement technique.

3.2. Residual stresses

Residual stresses are an important feature of the functional surface impairing the lifetime of a mechanical component. Residual stresses of the AD coatings have not been characterised in this work for two main reasons:

- the context of the proposed work concerns the processing of thick coatings obtained by CS or LC. This means that the coated part will never be used as-deposited but will be functional only once its surface has been machined;
- in our earlier study [46], the present authors showed that once a finish turning operation is applied, according to the selected depth of cut (0.3mm), the main affected depth of the coating is removed which will result in a new affected functional surface. The history of the deposition process can therefore be neglected as the residual stress state will directly depend on the last process applied.

The Figure 9 shows that FT can induce tensile residual stresses up to 150MPa into the first 5 to 15μm in both axial and tangential directions, followed by a compression peak close to -300MPa around 40μm. The profile is then progressively reaching -130MPa which has been shown to be the residual stress level of the AD CS coating at this depth [46].

Ball-burnishing is able to change the residual stress profile left by the finish turning into a compressive one. -50MPa can be achieved at the top surface which progressively decreases to -200MPa along the first 200μm below the surface, showing a potential deeper effect compared to FT. One can also notice that axial and tangential stresses are really close in magnitude all along the depth compared to FT. Due to the material removal itself, FT certainly applies anisotropic loadings onto the machined surface leading to this residual stress profile.

In LC, residual stresses were first investigated in FT but checking the potential influence of the selected heat treatment (HT). FT was thus applied on some raw AD and some heat-treated AD samples. Interestingly, surface tensile stresses were found to be really close whereas compressive stresses beyond 20μm were slightly larger after HT that on the raw AD coating (Fig. 10). The heat treatment does not finally drastically affect the stress distribution within the near-surface which is mainly affect by the last finish turning operation.

Applying a further ball-burnishing operation completely modify the residual stress profile as shown in Figure 11. The post-processing technique results in deep and intense compressive stresses almost reaching -1GPa at around 25μm from the surface in the axial direction. Whereas the effect of FT appears to be limited to 100μm, BB is able to affect up to 300μm of the near-surface region. These findings are consistent with the experimental results presented in [48, 51, 52] as well as the theoretical studies conducted by Yen et al. [53] or Kermouche et al. [54] using a finite element model.

Finally, the large difference in amplitude between the axial and tangential stresses along the first 100μm in BB proves that this process has a high anisotropic effect on the treated surface.

3.3. Comparison between CS and LC

From a microstructural point of view, both CS and LC deposition processes exhibited a modification of their as-deposited microstructure in the near-surface region on a depth of approximately 5 to 20μm once FT and BB were applied. If the generated LC microstructure appears closer to those obtained by Mondelin et al. [51] on a bulk 15-5PH martensitic stainless steel after FT, those on the CS samples are a bit specific considering the particular cohered particle type of microstructure. Indeed, not only the material within the particles is affected by the selected post-processing technique but also the inter-particles boundaries which are found to disappear by deformation and compression of the neighbouring particles. Material removal or deformation of a CS microstructure can almost be considered as post-treating a granular material due to the intrinsic nature of the CS deposit while the LC coating appears to be closer to a bulk material.

An interesting finding concerns the residual stress state within the two coatings. The latter are plotted side by side in the Figure 12 using the same scale on both axis and reveal the following aspects:

- after FT, stresses induced in the LC coatings are moderately larger in magnitude compared to those in the CS deposit, especially in the tangential direction;
- after FT and BB, the CS coating exhibit significantly lower compressive stresses compared to the cladded material. Stresses in both directions are similar whereas the difference between the stresses in the axial and tangential direction is more pronounced in the LC coating;
- the effect of BB after FT is relatively limited in the material deposited by CS whereas it is clearly predominant in LC.

As discussed in the previous section, the stress distribution observed in the LC coating after FT and FT+BB is consistent with those reported by Mondelin et al. [51] and Chomienne et al. [48] on a bulk 15-5PH. The authors highlighted surface tensile stresses between 300 and 500MPa after FT whereas BB led to surface stresses between -300 and -600MPa with a compression peak exceeding 1GPa [48]. Similar results with BB were found on a bulk 17-4PH by Zhang et al. [52]. This tends to show that the 17-4PH LC coating presents a behaviour similar to a bulk hot rolled martensitic stainless steel.

On the contrary, the different evolutions observed in the CS coating confirm that the behaviour of a CS type of microstructure is completely different from the similar bulk material. A tentative explanation could be the specific mechanisms occurring when cutting or ball-burnishing a cohered particle based material. The Figure 13a shows that after FT not only the bulk microstructure of a particle is deformed but also the inter-particle boundaries. Those are still open beyond 2 to 3μm from the top surface whereas they completely disappeared within the first 2μm. In the Figure 13b, one can noticed that after applying BB, the inter-particle boundaries got closed and completely disappeared all along the depth of the deposit.

This deformation phenomena occurring at the inter-particle boundaries could explain the lower compressive stresses achieved in the CS coating compared to the LC one. Indeed, part of the energy induced by the BB operation is in fact dissipated in deforming and compressing the inter-particle boundaries in the near surface instead of plastically deforming the bulk material. The lack of knowledge regarding residual stress distributions induced in CS martensitic stainless steel coatings impairs the validation of this statement and does not make possible the comparison with previously obtained data from the literature.

4. Conclusions

This paper focused on the effect of a finish turning and ball-burnishing operations on the surface and near surface properties of thick 17-4PH coatings. Two deposition processes have been investigated: Cold

Spray and Laser Cladding. The important findings of this work are as follows:

- Both deposited materials could be machined without any damage using the same cutting conditions as for a rolled bulk 17-4PH stainless steel;
- Applying a finish turning or ball-burnishing operation affected the near-surface microstructure resulting in a 5 to 10μm thick transformed layer in both deposits. The inter-particle boundaries of the cold spray coating were severely deformed with an orientation directed towards the material removal/deformation direction;
- A slight increase in the micro-hardness has been observed around these layers but more local measurements should be performed to specifically extract their mechanical properties;
- Tensile residual stresses were induced along the first 15 to 20μm by the finish turning operation in both cold spray and laser cladding coatings followed by a compression state. Larger amplitudes were reached in the cladded material with surface tangential stresses exceeding 400MPa and a compression peak up to -400MPa against -300MPa in cold spray;
- Applying or not a heat treatment to the cladded material did not change drastically the effect of the finish turning operation leading to a very similar residual stress distribution;
- Ball-burnishing improved the surface integrity of both deposited materials by changing the surface tensile stresses into compressive residual ones. The affected depth of this process could reach 300μm in the cladded material with deep and intense stresses down to -1GPa. However, the effect of ball-burnishing was found to be more limited in the cold spray coating with compressive stresses limited to -200MPa.

The last observation presents an interesting perspective as the reported differences on the residual stress distribution between the cold spray and cladded material highlight a different deformation mechanism. It is thus assumed that cohered particle type of microstructures do not behave as bulk ones, especially due to the inter-particle boundaries which play an important role. Further investigations should be performed to fully understand the local mechanism behind and also clarify the microstructural evolutions observed in the near region.

Acknowledgements

The authors would like to thank M. Fournier, Pierquet, Meynard, Thinard and Ranc for their help in carrying out part of the experiments and analyses. They also want to especially acknowledge the contribution of L. Thivillon from AG TOLERIE in carrying out the cladding experiments.

[1] K. Holmberg, A. Matthews, H. Ronkainen, Coatings tribology - contact mechanisms and surface design, Tribology International 31 (1998) 107 – 120.

[2] C. Navas, R. ColaÃğo, J. de Damborenea, R. Vilar, Abrasive wear behaviour of laser clad and flame sprayed-melted nicrbsi coatings, Surface and Coatings Technology 200 (2006) 6854 – 6862.

[3] W. Liu, Y. Hou, C. Liu, Y. Wang, R. Jiang, G. Xu, Hot corrosion behavior of a centimeter fe-based amorphous composite coating prepared by laser cladding in molten na2so4+k2so4 salts, Surface and Coatings Technology 270 (2015) 33 – 38.

[4] R. Sivakumar, B. Mordike, High temperature coatings for gas turbine blades: A review, Surface and Coatings Technology 37 (1989) 139 – 160.

[5] Y. Chew, J. H. L. Pang, G. Bi, B. Song, Effects of laser cladding on fatigue performance of aisi 4340 steel in the as-clad and machine treated conditions, Journal of Materials Processing Technology 243 (2017) 246 – 257.

[6] H. KÃűhler, K. Partes, J. R. Kornmeier, F. Vollertsen, Residual stresses in steel specimens induced by laser cladding and their effect on fatigue strength, Physics Procedia 39 (2012) 354 – 361. Laser Assisted Net shape Engineering 7 (LANE 2012).

[7] Z. Bergant, U. Trdan, J. Grum, Effect of high-temperature furnace treatment on the microstructure and corrosion behavior of nicrbsi flame-sprayed coatings, Corrosion Science 88 (2014) 372 – 386.

[8] J. Tan, L. Looney, M. Hashmi, Component repair using hvof thermal spraying, Journal of Materials Processing Technology 92-93 (1999) 203 – 208.

[9] P. F. Mendez, N. Barnes, K. Bell, S. D. Borle, S. S. Gajapathi, S. D. Guest, H. Izadi, A. K. Gol, G. Wood, Welding processes for wear resistant overlays, Journal of Manufacturing Processes 16 (2014) 4 – 25. Recent Developments in Welding Processes.

[10] L. Pawlowski, Thick laser coatings: A review, Journal of Thermal Spray Technology 8 (1999) 279–295.

[11] I. Smurov, M. Doubenskaia, A. Zaitsev, Comprehensive analysis of laser cladding by means of optical diagnostics and numerical simulation, Surface and Coatings Technology 220 (2013) 112 – 121. Proceedings of the fifth workshop RIPT (Les Rencontres Internationales sur la Projection Thermique).

[12] W. Li, K. Yang, S. Yin, X. Yang, Y. Xu, R. Lupoi, Solid-state additive manufacturing and repairing by cold spraying: A review, Journal of Materials Science & Technology 34 (2018) 440 – 457.

[13] S. Yin, P. Cavaliere, B. Aldwell, R. Jenkins, H. Liao, W. Li, R. Lupoi, Cold spray additive manufacturing and repair: Fundamentals and applications, Additive Manufacturing 21 (2018) 628 – 650.

[14] I. Smurov, Laser cladding and laser assisted direct manufacturing, Surface and Coatings Technology 202 (2008) 4496 – 4502. 3 Rencontres Internationales de la Projection Thermique.

[15] S. M. Thompson, L. Bian, N. Shamsaei, A. Yadollahi, An overview of direct laser deposition for additive manufacturing; part i: Transport phenomena, modeling and diagnostics, Additive Manufacturing 8 (2015) 36 – 62.

[16] J.-Y. Chen, K. Conlon, L. Xue, R. Rogge, Experimental study of residual stresses in laser clad aisi p20 tool steel on pre-hardened wrought p20 substrate, Materials Science and Engineering: A 527 (2010) 7265 – 7273.

[17] S. Paul, K. Thool, R. Singh, I. Samajdar, W. Yan, Experimental characterization of clad microstructure and its correlation with residual stresses, Procedia Manufacturing 10 (2017) 804 – 818. 45th SME North American Manufacturing Research Conference, NAMRC 45, LA, USA.

[18] R. R. Rashid, S. Abaspour, S. Palanisamy, N. Matthews, M. Dargusch, Metallurgical and geometrical characterisation of the 316l stainless steel clad deposited on a mild steel substrate, Surface and Coatings Technology 327 (2017) 174 – 184.

[19] M. J. Marques, A. Ramasamy, A. C. Batista, J. P. Nobre, A. Loureiro, Effect of heat treatment on microstructure and residual stress fields of a weld multilayer austenitic steel clad, Journal of Materials Processing Technology 222 (2015) 52 – 60.

[20] A. Papyrin, Cold spray technology, Advanced Materials and Processes 159 (2001) 49–51.

[21] S. Grigoriev, A. Okunkova, A. Sova, P. Bertrand, I. Smurov, Cold spraying: From process fundamentals towards advanced applications, Surface and Coatings Technology 268 (2015) 77 – 84. 6th Rencontres Internationales de la Projection Thermique.

[22] T. Schmidt, H. Assadi, F. GÃďrtner, H. Richter, T. Stoltenhoff, H. Kreye, T. Klassen, From particle acceleration to impact and bonding in cold spraying, Journal of Thermal Spray Technology 18 (2009) 794–808.

[23] H. Assadi, F. GÃďrtner, T. Stoltenhoff, H. Kreye, Bonding mechanism in cold gas spraying, Acta Materialia 51 (2003) 4379–4394.

[24] V. Luzin, K. Spencer, M.-X. Zhang, Residual stress and thermo-mechanical properties of cold spray metal coatings, Acta Materialia 59 (2011) 1259 – 1270.

[25] F. Liu, Y. Mao, X. Lin, B. Zhou, T. Qian, Microstructure and high temperature oxidation resistance of ti-ni gradient coating on ta2 titanium alloy fabricated by laser cladding, Optics & Laser Technology 83 (2016) 140 – 147.

[26] A. Yakovlev, E. Trunova, D. Grevey, M. Pilloz, I. Smurov, Laser-assisted direct manufacturing of functionally graded 3d objects, Surface and Coatings Technology 190 (2005) 15 – 24.

[27] S. Klinkov, V. Kosarev, A. Sova, I. Smurov, Deposition of multicomponent coatings by cold spray, Surface and Coatings Technology 202 (2008) 5858 – 5862.

[28] O. Tazegul, V. Dylmishi, H. Cimenoglu, Copper matrix composite coatings produced by cold spraying process for electrical applications, Archives of Civil and Mechanical Engineering 16 (2016) 344 – 350.

[29] H. Liu, J. Hao, Z. Han, G. Yu, X. He, H. Yang, Microstructural evolution and bonding characteristic in multi-layer laser cladding of nicocr alloy on compacted graphite cast iron, Journal of Materials Processing Technology 232 (2016) 153 – 164.

[30] Y. Xu, M. Chirol, C. Li, A. Vardelle, Formation of al2o3 diffusion barrier in cold-sprayed nicocraly/ni multi-layered coatings on 304ss substrate, Surface and Coatings Technology 307 (2016) 603 – 609.

[31] R. Blose, B. Walker, R. Walker, S. Froes, New opportunities to use cold spray process for applying additive features to titanium alloys, Metal Powder Report 61 (2006) 30 – 37.

[32] J. Pattison, S. Celotto, R. Morgan, M. Bray, W. OâĂŹNeill., Cold gas dynamic manufacturing: A non-thermal approach to freeform fabrication, International Journal of Machine Tools and Manufacture 47 (2007) 627 – 634.

[33] S. Yin, P. Cavaliere, B. Aldwell, R. Jenkins, H. Liao, W. Li, R. Lupoi, Cold spray additive manufacturing and repair: Fundamentals and applications, Additive Manufacturing 21 (2018) 628 – 650.

[34] S. Bagherifard, S. Monti, M. V. Zuccoli, M. Riccio, J. Kondas, M. Guagliano, Cold spray deposition for additive manufacturing of freeform structural components compared to selective laser melting, Materials Science and Engineering: A 721 (2018) 339 – 350.

[35] M. Jeandin, Cold spray under the banner of thermal spray in the whirlwind of additive manufacturing, Surface Engineering 34 (2018) 341–343.

[36] B. Dutta, S. Palaniswamy, J. Choi, L. Song, J. Mazumder, Additive manufacturing by direct metal deposition, Advanced Materials and Processes 169 (2011) 33–36.

[37] D. Kotoban, A.Nazarov, I. Shishkovsky, Comparative study of selective laser melting and direct laser metal deposition of ni3al intermetallic alloy, Procedia IUTAM 23 (2017) 138 – 146. IUTAM Symposium on Growing solids, 23-27 June 2015, Moscow, Russia.

[38] P. Ghosal, M. Majumder, A. Chattopadhyay, Study on direct laser metal deposition, Materials Today: Proceedings 5 (2018) 12509 – 12518. International Conference on Materials Manufacturing and Modelling, ICMMM - 2017, 9 - 11, March 2017.

[39] S. Sun, Q. Liu, M. Brandt, V. Luzin, R. Cottam, M. Janardhana, G. Clark, Effect of laser clad repair on the fatigue behaviour of ultra-high strength aisi 4340 steel, Materials Science and Engineering: A 606 (2014) 46 – 57.

[40] A. Sova, S. Grigoriev, A. Okunkova, I. Smurov, Cold spray deposition of 316l stainless steel coatings on aluminium surface with following laser post-treatment, Surface and Coatings Technology 235 (2013) 283 – 289.

[41] K. Luo, X. Jing, J. Sheng, G. Sun, Z. Yan, J. Lu, Characterization and analyses on micro-hardness, residual stress and microstructure in laser cladding coating of 316l stainless steel subjected to massive lsp treatment, Journal of Alloys and Compounds 673 (2016) 158 – 169.

[42] H. KÃűhler, R. Rajput, P. Khazan, J. R. Kornmeier, On the influence of laser cladding and post-processing strategies on residual stresses in steel specimens, Physics Procedia 56 (2014) 250 – 261. 8th International Conference on Laser Assisted Net Shape Engineering LANE 2014.

[43] P. Zhang, Z. Liu, Y. Guo, Machinability for dry turning of laser cladded parts with conventional vs. wiper insert, Journal of Manufacturing Processes 28 (2017) 494 – 499. SI: NAMRC 45.

[44] P. Zhang, Z. Liu, Effect of sequential turning and burnishing on the surface integrity of crâĂŞni-based stainless steel formed by laser cladding process, Surface and Coatings Technology 276 (2015) 327 – 335.

[45] P. Zhang, Z. Liu, Enhancing surface integrity and corrosion resistance of laser cladded crâĂŞni alloys by hard turning and low plasticity burnishing, Applied Surface Science 409 (2017) 169 – 178.

[46] A. Sova, C. Courbon, F.Valiorgue, J.Rech, Ph.Bertrand, Effect of turning and ball burnishing on the microstructure and residual stress distribution in stainless steel cold spray deposits, Journal of Thermal Spray Technology 26 (2017) 1922–1934.

[47] H. Assadi, H. Kreye, F. GÃďrtner, T. Klassen, Cold spraying âĂŞ a materials perspective, Acta Materialia 116 (2016) 382 – 407.

[48] V. Chomienne, F. Valiorgue, J. Rech, C. Verdu, Influence of ball burnishing on residual stress profile of a 15-5ph stainless steel, CIRP Journal of Manufacturing Science and Technology 13 (2016) 90–96.

[49] M. A. Meyers, Y. B. Xu, Q. Xue, M. T. PÃľrez-Prado, T. R. McNelley, Microstructural evolution in adiabatic shear localization in stainless steel, Acta Materialia 51 (2003) 1307 – 1325.

[50] H. Beladi, G. L. Kelly, P. D. Hodgson, Ultrafine grained structure formation in steels using dynamic strain induced transformation processing, International Materials Reviews 52 (2007) 14 – 28.

[51] A. Mondelin, F. Valiorgue, J. Rech, M. Coret, E. Feulvarch, Hybrid model for the prediction of residual stresses induced by 15-5ph steel turning, International Journal of Mechanical Sciences 58 (2012) 69 – 85.

[52] T. Zhang, N. Bugtai, I. Marinescu, Burnishing of aerospace alloy: A theoreticalâĂŞexperimental approach, Journal of Manufacturing Systems 37 (2015) 472 – 478.

[53] Y. Yen, P. Sartkulvanich, T. Altan, Finite element modeling of roller burnishing process, CIRP Annals 54 (2005) 237 – 240.

[54] G. Kermouche, J. Rech, H. Hamdi, J. Bergheau, On the residual stress field induced by a scratching round abrasive grain, Wear 269 (2010) 86 – 92.

List of Tables

Nomenclature

AD	As deposited	SEM	Scanning Electron Microscope
BB	Ball burnishing	XRD	X-Ray Diffraction
CS	Cold Spray	Vc	Cutting speed
$EBSD$	Electron BackScatter Diffraction	ap	Depth of cut
FT	Finish turning operation	f	Feed rate
HT	Stress relief heat treatment	β	Incidence angle of the beam
$HVOF$	High Velocity Oxy-Fuel	λ	Wavelength of the incident beam
LC	Laser Cladding	θ	Angle of the diffracted beam

Parameter	Unit	Value
Gas stagnation pressure	MPa	4
Gas stagnation temperatur	$°C$	650
Spraying distance	mm	40
Substrate rotation speed	rpm	12
Nozzle displacement speed relatively to the cylinder axis	mm/s	0.5
Nozzle traverse speed relatively to the surface	mm/s	390
Number of nozzle passes	-	2
Powder feed rate	g/s	approx. 1.3

Table 1 — Cold spray spraying parameters.

Parameter	Unit	Value
Beam sport diameter	mm	6
Laser cladding speed	m/min	0.8
Laser power	kW	4
Powder feeding rate	g/min	24
Coating thickness	mm	1.5

Table 2 — Laser cladding deposition parameters.

List of Figures

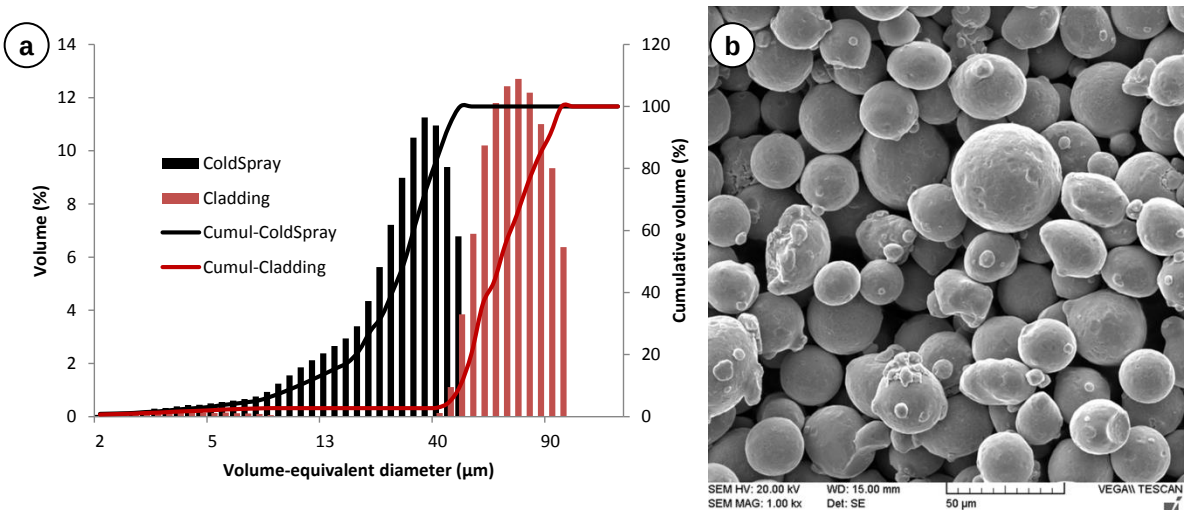

Fig. 1 — Particle size distribution of the 17-4 PH stainless steel powder used for each deposition process (a) and SEM image of particles (b) of the powder employed in CS.

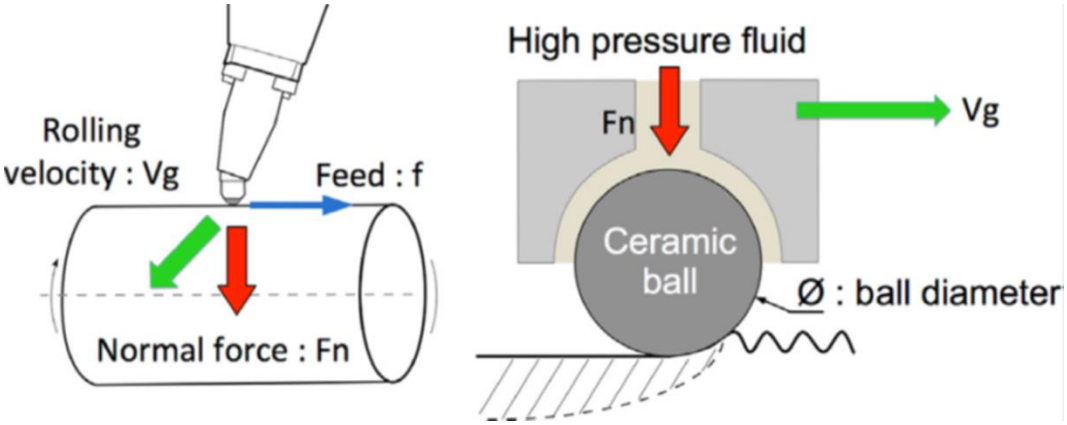

Fig. 2 — Principle of the ball burnishing process [48]

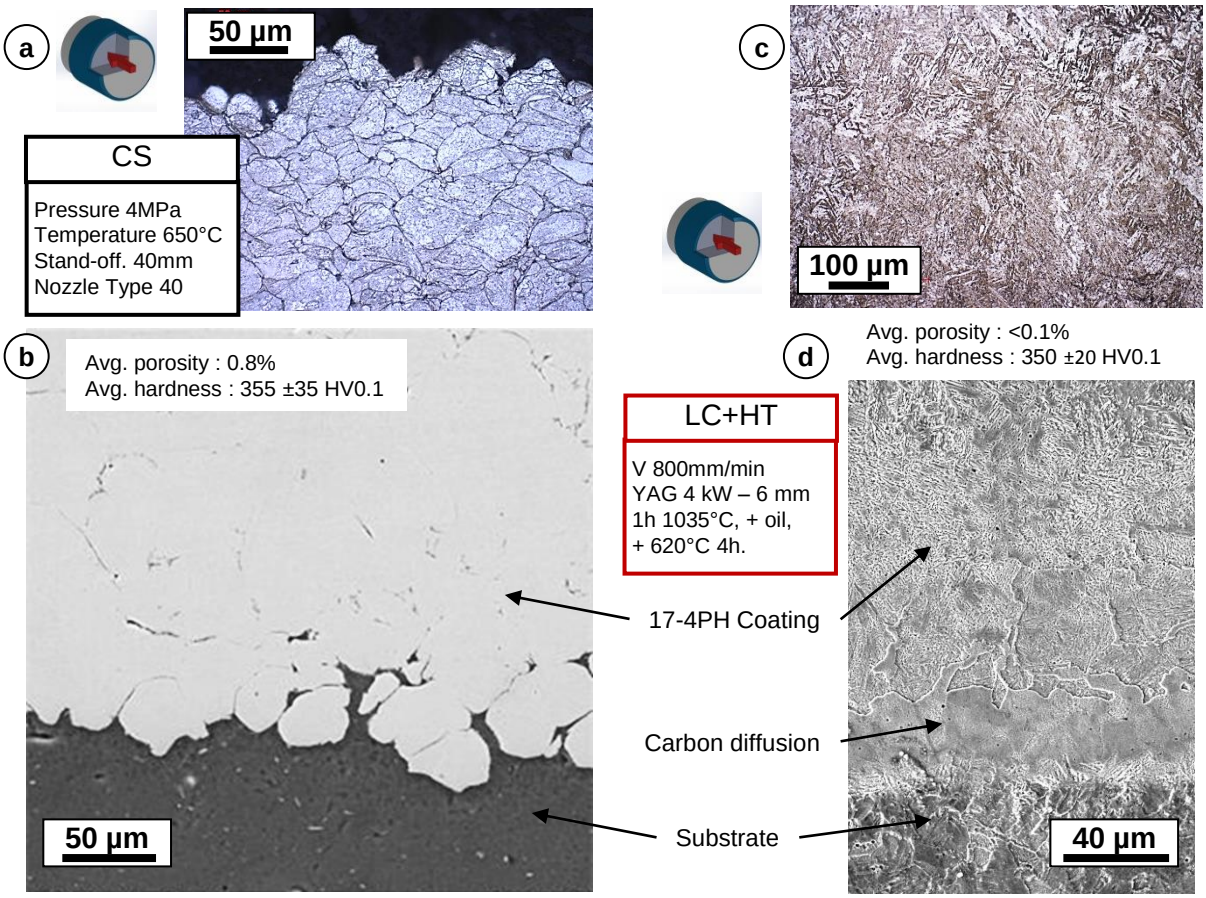

Fig. 3 — Optical image of the as-deposited (AD) coating top surface and SEM image of the substrate/coating interface in CS a,b) and LC c,d)

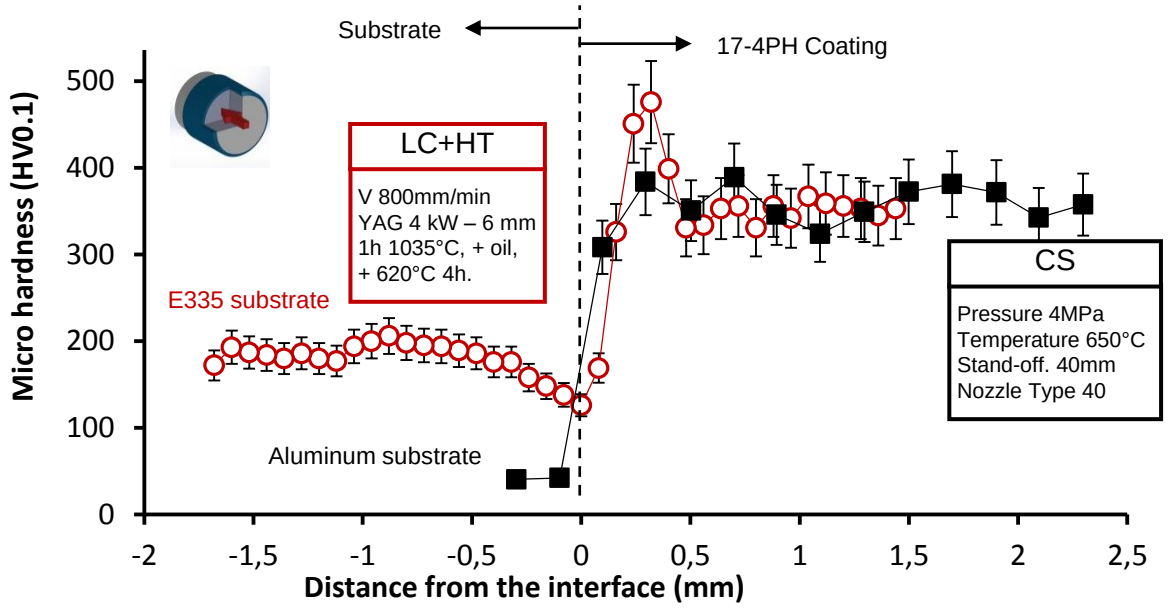

Fig. 4 — Microhardness profiles measured on the AD coatings

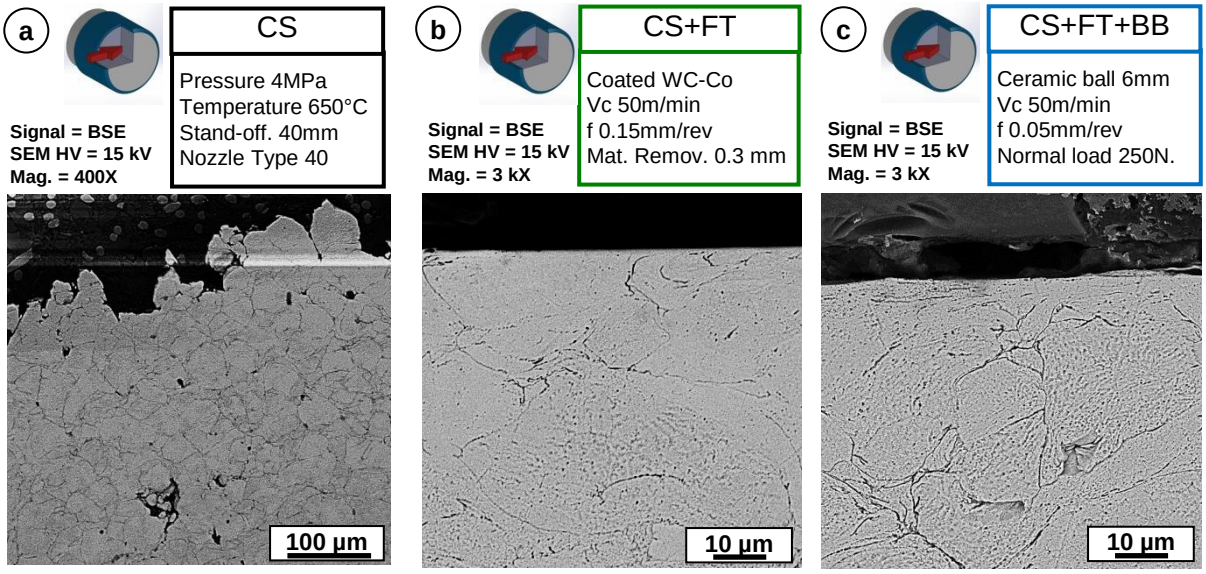

Fig. 5 — SEM images of a) the AD CS coating cross section, b) after finish turning and c) after finish turning and ball burnishing taken along the parallel direction relative to the substrate axis

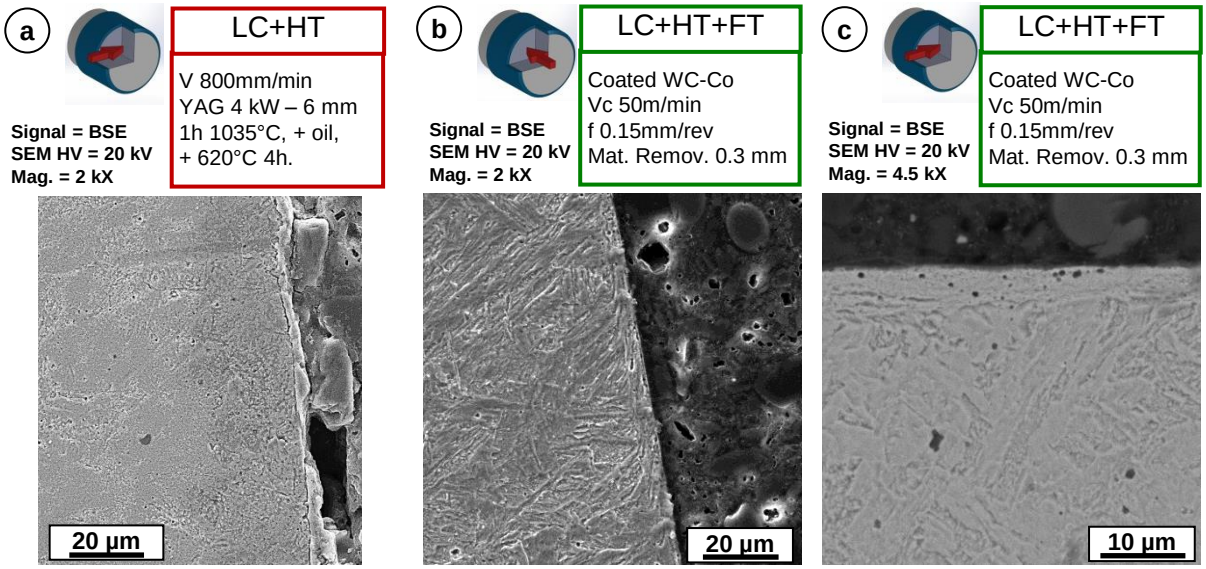

Fig. 6 — SEM images of a) the AD LC coating cross section, b) after finish turning along the perpendicular and c) parallel direction relative to the substrate axis

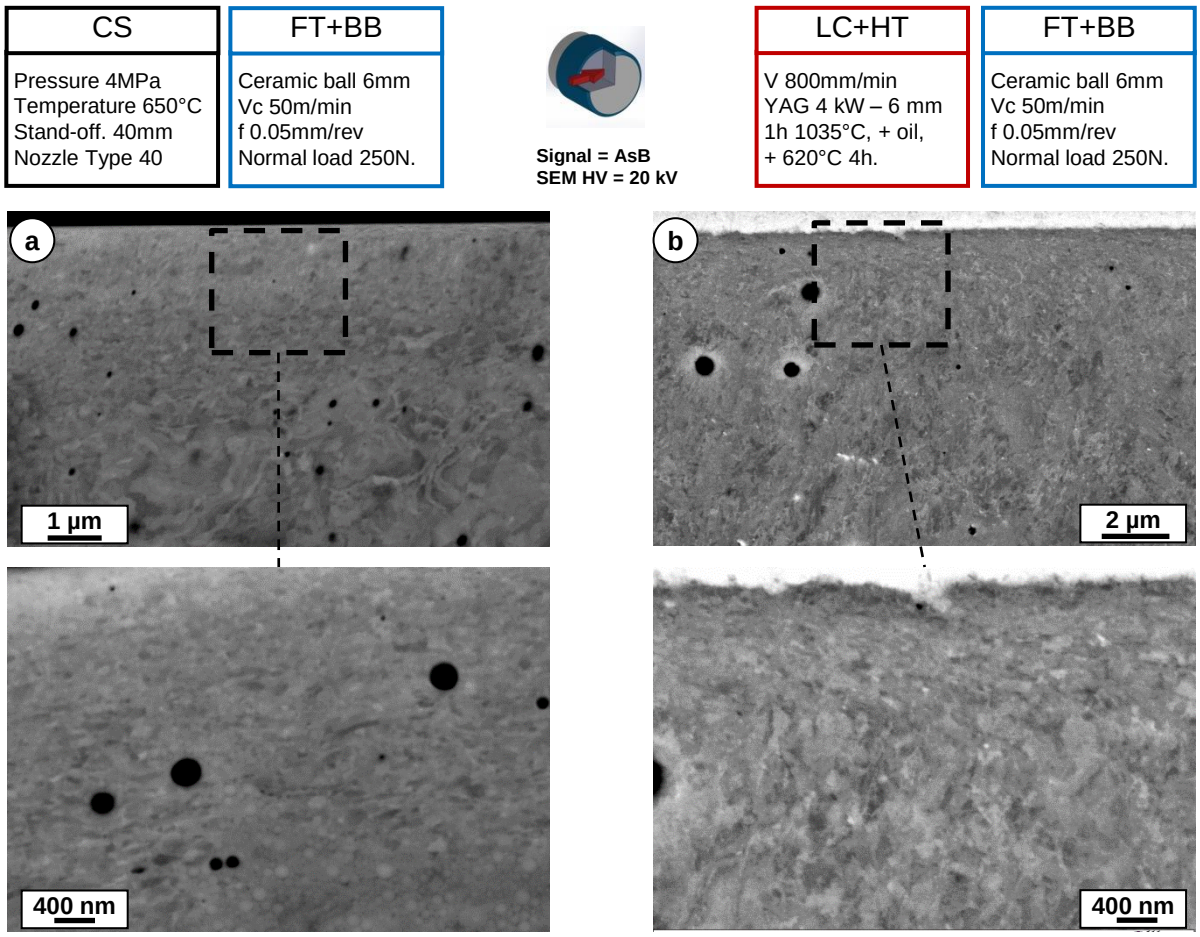

Fig. 7 — High resolution SEM images of a) the CS coating cross section, b) the LC coating both after finish turning and ball burnishing taken along the parallel direction relative to the substrate axis

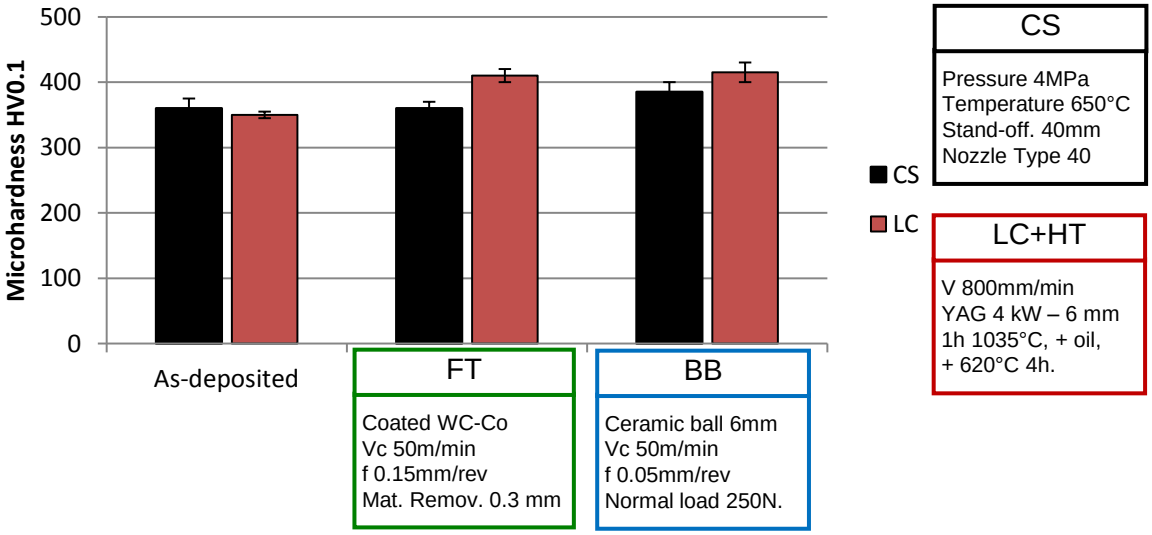

Fig. 8 — Comparison of the near-surface microhardness on the as deposited samples, after turning and after turning and ball-burnishing

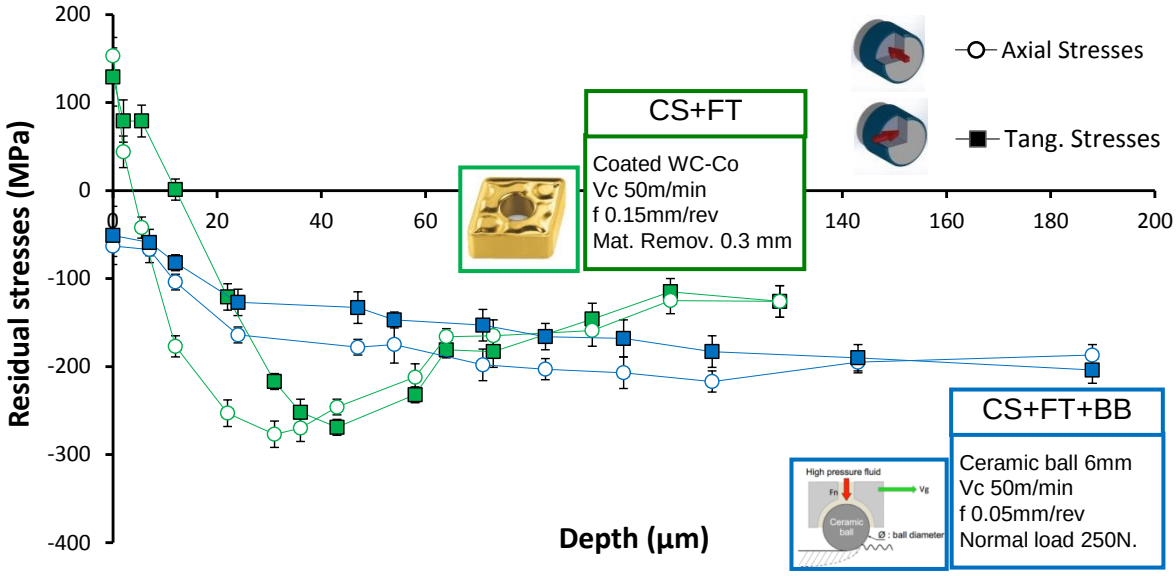

Fig. 9 — Residual stress profiles of the CS coating after finish turning (FT) and finish turning followed by ball-burnishing (BB)

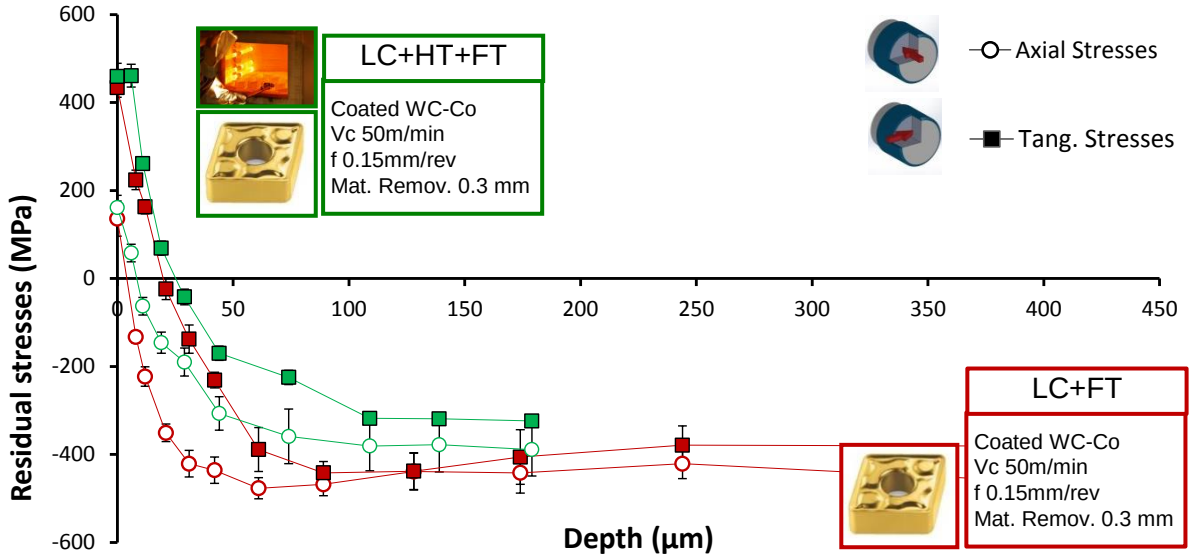

Fig. 10 — Residual stress profiles of the LC coating after finish turning (FT) on the as-deposited coating and as-deposited followed by heat treatment (HT)

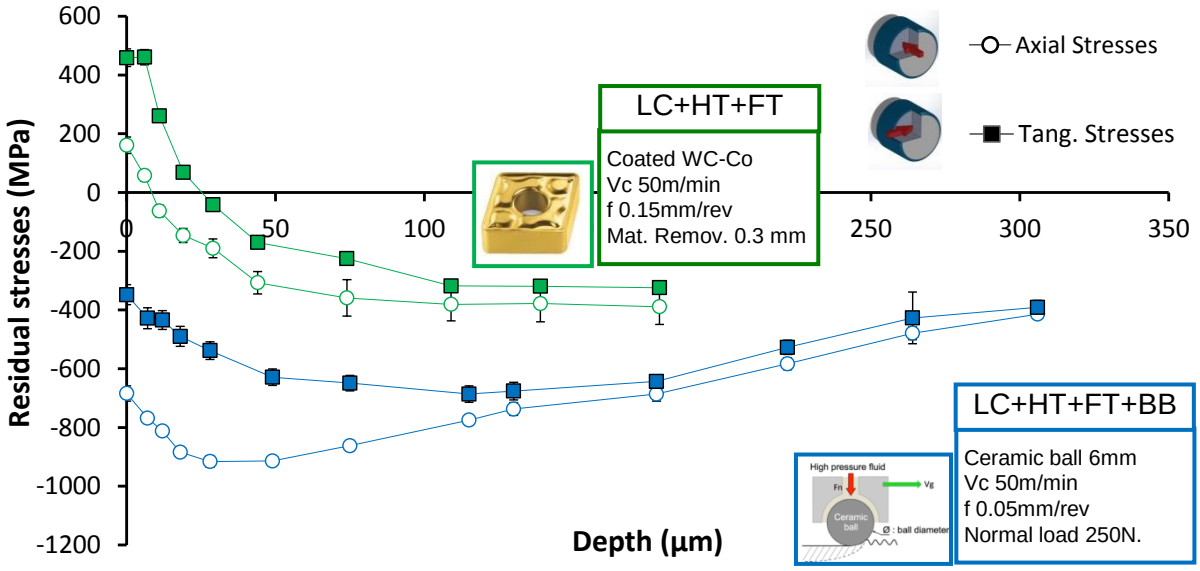

Fig. 11 — Residual stress profiles of the LC coating after finish turning (FT) and finish turning followed by ball-burnishing (BB)

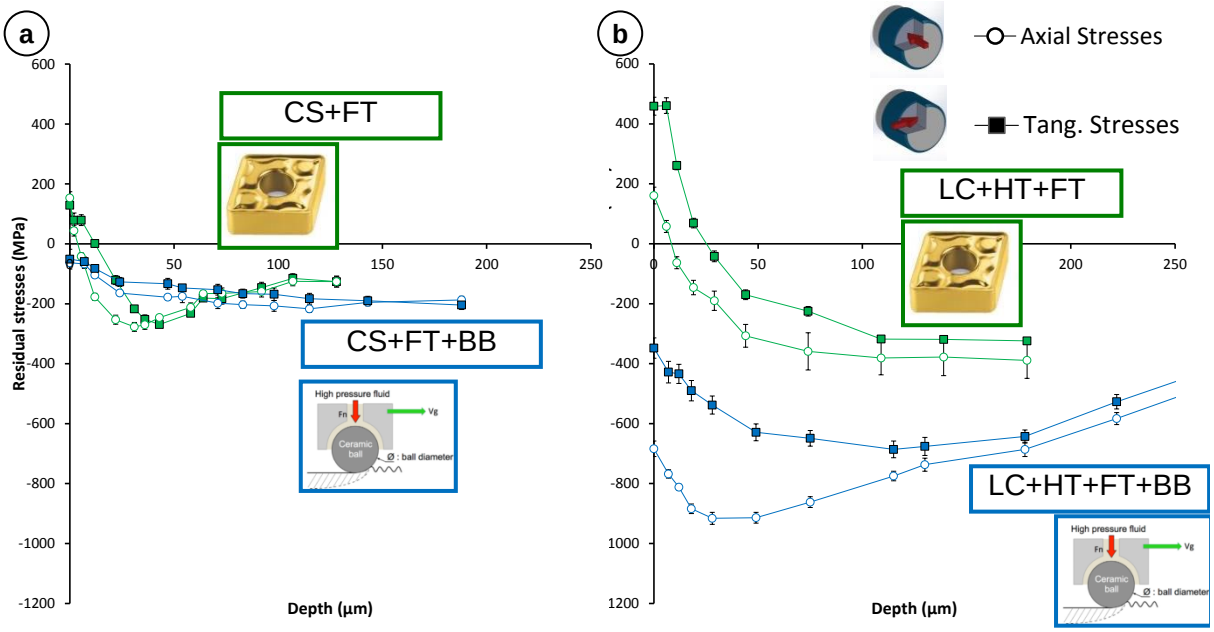

Fig. 12 — Comparison between the residual stress profiles of the a) CS and b) LC coatings after finish turning (FT) and finish turning followed by ball-burnishing (BB)

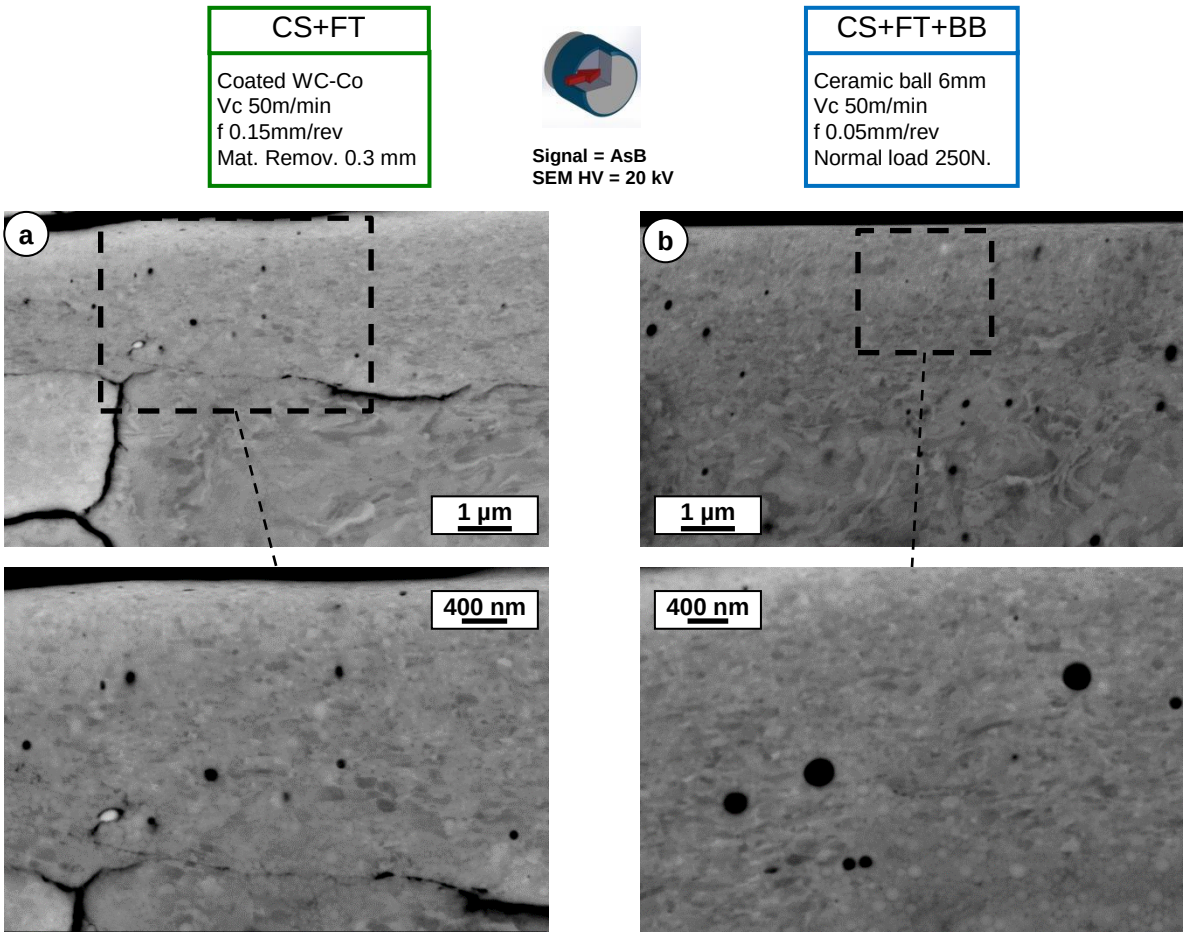

Fig. 13 — High resolution SEM images of a) the CS coating cross section after finish turning, b) after finish turning and ball burnishing taken along the parallel direction relative to the substrate axis